Experimental Characterization and Modeling of Twin-Screw Extruder Elements for Pharmaceutical Hot Melt Extrusion

Andreas Eitzlmayr and Johannes Khinast
Institute for Process and Particle Engineering, Graz University of Technology, Inffeldgasse 13/III, 8010 Graz, Austria

Gudrun Hörl and Gerold Koscher
Research Center Pharmaceutical Engineering GmbH, Inffeldgasse 13/III, 8010 Graz, Austria

Gavin Reynolds, Zhenyu Huang, Jonathan Booth, and Philip Shering
Pharmaceutical Development, AstraZeneca, Charter Way, Macclesfield, SK10 2NA, U.K.

DOI 10.1002/aic.14184
Published online July 24, 2013 in Wiley Online Library (wileyonlinelibrary.com)

In this study we characterized various screw elements of a co-rotating twin-screw extruder used for pharmaceutical hot melt extrusion (HME) and measured the pressure characteristic, i.e., the correlation between the axial pressure gradient and the material throughput in a completely filled screw section at different screw speeds. A typical HME matrix material, Soluplus, was used for the experiments and its required rheological properties were determined. A three-parameter model based on a dimensionless formulation of the measured quantities was used. These parameters could not be determined uniquely by fitting to experimental data. Therefore we developed an approach to approximate one empirical parameter based on the mechanistic consideration of a pressure-driven channel flow. The model was extended to account for the variable melt temperature. The results confirmed the expected tendencies and established an essential input parameter set for one-dimensional simulations of co-rotating twin-screw extruders. © 2013 American Institute of Chemical Engineers *AIChE J*, 59: 4440–4450, 2013
Keywords: hot melt extrusion, screw element, pressure characteristic, rheology, soluplus

Introduction

Hot melt extrusion (HME) has been used for many decades in various industries (e.g., plastics and food) and, in recent years, has become an important pharmaceutical manufacturing operation.[1] Extrusion is defined as the process of forcing a material through a die under controlled conditions and high pressure. HME applies temperature levels above the melting (or softening) point in order to extrude the material in a viscous state.[2] In pharmaceutical manufacturing, HME can potentially increase the bioavailability of poorly soluble drugs,[3] form solid solutions and amorphous solid dispersions[4] and enhance the product quality due to the mixing efficiency of extruders.[2] Moreover, in a single step raw materials can be converted into a final delivery form, for example, through calandering.

Screw extruders (single-, twin-, and multi-screw) are the most common extrusion devices,[1] which combine various process steps such as mixing, melting, conveying, degassing, and dissolution of particles in a single device. These properties increase the manufacturing efficiency and reduce operation costs.[2] In pharmaceutical manufacturing, typically co-rotating twin-screw extruders with self-cleaning screws and modular screw design are used, that is, the screws are divided into different types of screw elements (e.g., conveying elements and kneading elements), which can be individually arranged to accommodate actual process requirements. While this feature offers high flexibility, achieving optimal process conditions is a challenge as developing optimal screw configurations requires experience and/or experimental work based on trial and error.

Mechanistic models can provide useful insights into the effects of various screw configurations, improve understanding of the underlying mechanisms, and reduce the experimental and empirical effort. Although different models describing the flow field in screw extruders have been developed, not all aspects of the extrusion process can be predicted in detail. For example, to date no detailed methods exist for the simulation of the flow in partially filled screws. The involved physical phenomena (non-Newtonian flow, wall slip, small gaps, free surfaces, etc.) are highly complex and first-principle design methods are not available.[5]

Existing mechanistic models of the entire HME process are based on one-dimensional (1-D) models of the flow along co-rotating twin screws, resolving the pressure and filling ratio along the screw axis.[6–9] These models basically account for the pressure-throughput correlation of single screw elements, describing the pressure gradient vs. flow rate in completely filled screw sections.[5,10–14] The resulting predictions of the material transport along the screw have been used to develop

J. Khinast is also affliated with Research Center Pharmaceutical Engineering GmbH, Inffeldgasse 13/III, 8010 Graz, Austria.

Correspondence concerning this article should be addressed to J. Khinast at khinast@tugraz.at.

models of the residence time distribution in extruders.[15–19] In recent years, this approach has been extended to models of reactive extrusion.[20–22] Spatially resolved simulations of the flow field in completely filled screw sections have been performed using computational fluid dynamics (CFD),[14,23–28] but they cannot be applied to an entire twin screw due to the required calculation effort and the challenge of partially filled screw sections in three-dimensional (3-D) simulations. Thus, simplified descriptions of extrusion processes are still prevalent.

Pawlowski[10] showed that for single screw extruders and Newtonian fluids in the creeping flow regime, the axial pressure gradient is linearly correlated with the throughput, and described the correlation by an empirical model termed "pressure characteristic", based on dimensionless numbers. As the pressure characteristic is determined by the detailed screw geometry, the used empirical parameters are called "screw parameters". Kohlgrüber and Wiedmann[5] applied this concept to co-rotating twin-screw extruders and extended it to shear-thinning polymer melts described by the Carreau model.

In our work, we developed a 1-D simulation for co-rotating twin-screw extruders based on the pressure-characteristic model by Kohlgrüber and Wiedmann[5]. To simulate a real extrusion process, screw parameters for all used screw elements must be provided as input parameters. Thus, we present pressure-characteristic measurements for different screw elements and the resulting screw parameters using Soluplus, a typical matrix material for pharmaceutical HME. The required temperature-dependent rheological material parameters of Soluplus have been measured. In the extrusion experiments, we found a slight variation of the melt temperature with the throughput, which is not negligible due to the strong temperature dependency of the viscosity. To account for this effect, the pressure characteristic was corrected for the temperature-dependence of the material parameters. Moreover, we developed an approach to estimate the empirical shear-rate parameter A_3 to overcome an underdetermined fitting problem. In summary, input parameters for the 1-D simulation of co-rotating twin-screw extruders were established.

Mathematical Model

Pressure-characteristic model

The description of Pawlowski[10] and Kohlgrüber and Wiedmann[5] is based on a dimensionless formulation of the volumetric throughput and the axial pressure gradient in completely filled screw sections (similarly to Ref. 11), where the dimensionless throughput $\dot{V}^*$ is defined as the volumetric throughput $\dot{V}$ over the screw speed n and the nominal screw diameter D cubed

$$\dot{V}^* = \frac{\dot{V}}{nD^3}. \tag{1}$$

For measurement purposes, the axial pressure gradient $\partial p/\partial x$ is approximated by the quotient of pressure difference and axial distance $\Delta p/\Delta x$ (see Figure 7). The dimensionless axial pressure gradient $\Delta p^*/\Delta x^*$ is defined using the dynamic viscosity of the material η, the screw speed n, and the nominal screw diameter D as follows

$$\left(\frac{\Delta p^*}{\Delta x^*}\right) = \frac{\Delta p}{\eta \cdot n} \cdot \frac{D}{\Delta x} \tag{2}$$

The correlation between dimensionless throughput $\dot{V}^*$ and dimensionless axial pressure gradient ($\Delta p^*/\Delta x^*$) is termed pressure characteristic. Using the described dimensionless quantities, Pawlowski[10] experimentally showed that the pressure characteristic of a certain screw element is invariant for different screw speeds n, screw diameters D, and viscosities η under the following conditions:

- Creeping flow, that is, sufficiently low Reynolds number $Re = \rho \cdot n \cdot D^2/\eta$ (ρ being the density). The limiting Reynolds number depends on the screw geometry. In a specific case ($D = 60$ mm), $Re < 100$ satisfied this condition.[10] Typically, high-viscosity materials used in HME generally lead to Reynolds numbers below 1 and, thus in technically relevant cases the creeping flow regime can be assumed.
- Newtonian fluid
- Geometrical similarity of the entire flow-relevant geometry.

Furthermore, it was demonstrated that for Newtonian fluids in the creeping flow regime, the pressure characteristic follows a linear function, which is described as[5,10]

$$\frac{\Delta p^*}{\Delta x^*} = \frac{\Delta p}{\eta \cdot n} \cdot \frac{D}{\Delta x} = A_2 \cdot \left(1 - \frac{\dot{V}^*}{A_1}\right) \tag{3}$$

where A_1 and A_2 are the screw parameters, that is, the axis intercepts of the linear function (i.e., $\Delta p^*/\Delta x^* = 0$ for $\dot{V}^* = A_1$ and $\Delta p^*/\Delta x^* = A_2$ for $\dot{V}^* = 0$). Thus, parameter A_1 represents the throughput in a completely filled screw section without back pressure (i.e., inherent conveying capacity), whereas A_2 represents the pressure gradient in a completely filled screw section conveying toward a closed die. An approximation for A_1 is given as[29]

$$A_1 \approx \frac{1}{2}\frac{A_{\mathrm{cr}} \cdot T_{\mathrm{S}}}{D^3} \tag{4}$$

where A_{cr} is a free cross-section area illustrated as a shaded area in Figure 2 and T_{S} is the screw pitch. In reality, typical materials used for HME are not Newtonian fluids but rather shear-thinning materials that can often be described via the Carreau model for constant temperature[5,30]

$$\eta(\dot{\gamma}) = \frac{\eta_0}{\left[1 + \frac{|\dot{\gamma}|}{\dot{\gamma}_{\mathrm{crit}}}\right]^m} \tag{5}$$

where η_0 is the zero-shear-rate viscosity, $\dot{\gamma}_{\mathrm{crit}}$ is the critical shear rate and m the Carreau exponent. Kohlgrüber and Wiedmann[5] extended the linear pressure characteristic for Newtonian fluids to non-Newtonian fluids described by the Carreau model. For this purpose, the Newtonian viscosity in Eq. 3 was substituted by Eq. 5

$$\frac{\Delta p^*}{\Delta x^*} = \frac{\Delta p}{\frac{\eta_0}{\left[1 + \frac{|\dot{\gamma}|}{\dot{\gamma}_{\mathrm{crit}}}\right]^m} \cdot n} \cdot \frac{D}{\Delta x} = A_2 \cdot \left(1 - \frac{\dot{V}^*}{A_1}\right) \tag{6}$$

Then the dimensionless axial pressure gradient was redefined for a Carreau fluid (indicated by index C) using the zero-shear-rate viscosity η_0 as

$$\frac{\Delta p_{C^*}}{\Delta + x^*} = \frac{\Delta p}{\eta_0 \cdot n} \cdot \frac{D}{\Delta x} = \frac{A_2 \cdot \left(1 - \frac{\dot{V}^*}{A_1}\right)}{\left[1 + \frac{|\dot{\gamma}|}{\dot{\gamma}_{\mathrm{crit}}}\right]^m} \tag{7}$$

This pressure-characteristic function is nonlinear and predicts lower pressure gradients compared to the linear function in the Newtonian case caused by the shear-thinning effect of

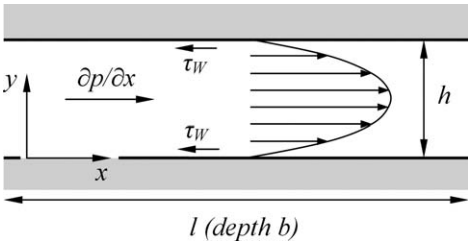

Figure 1. Two-plate model.

the melt. However, the issue of how to determine the shear rate $\dot{\gamma}$ is critical for a correct representation of the problem. In the real flow field around the screws, the shear rate varies strongly, for example, in the smallest gaps of $O(10^{-4}-10^{-3}$ m), higher shear rates can be expected than in the screw channels of $O(10^{-3}-10^{-2}$ m). Thus, using a single value for the shear rate in Eq. 7 ("representative shear rate" $\dot{\gamma}_r$) is a simplification. However, Kohlgrüber and Wiedmann[5] created a model that describes the representative shear rate proportional to the pressure-induced backflow $(1-\dot{V}^*/A_1)$. At the inherent conveying point $(\dot{V}^*=A_1)$, where no pressure-induced backflow occurs, the representative shear rate is zero. The representative shear rate increases with the increasing backflow. Furthermore, the shear rate is set to be proportional to the screw speed and an empirical fitting parameter A_3

$$\dot{\gamma}_r = A_3 \cdot n \cdot \left(1-\frac{\dot{V}^*}{A_1}\right) \tag{8}$$

Substituting this in Eq. 7 leads to the following pressure-characteristic function[5]

$$\frac{\Delta p_{C^*}}{\Delta x^*} = \frac{\Delta p}{\eta_0 \cdot n} \cdot \frac{D}{\Delta x} = \frac{A_2 \cdot \left(1-\frac{\dot{V}^*}{A_1}\right)}{\left[1+\frac{A_3 \cdot n}{\dot{\gamma}_{crit}} \cdot \left|1-\frac{\dot{V}^*}{A_1}\right|\right]^m} \tag{9}$$

Equation 9 can be used to fit the measured pressure gradients for shear-thinning fluids described by the Carreau model[5]. Kohlgrüber and Wiedmann[5] also presented a formulation equivalent to Eq. 9, which is based on the representative viscosity η_r (with $\eta_r=\eta(\dot{\gamma}_r)$ from Eq. 5 and $\dot{\gamma}_r$ from Eq. 8)

$$\frac{\Delta p^*}{\Delta x^*} = \frac{\Delta p}{\eta_r \cdot n} \cdot \frac{D}{\Delta x} = A_2 \cdot \left(1-\frac{\dot{V}^*}{A_1}\right) \tag{10}$$

Here, the shear-thinning effect is incorporated into the representative viscosity η_r, leading to a representation in which the measured data points of shear-thinning fluids are located along the linear pressure-characteristic function of Newtonian fluids.

Approximation of A_3

Our study showed that establishing the three screw parameters (A_1, A_2, A_3) by fitting the measured data leads to an underdetermined problem, that is, different combinations of A_1, A_2, and A_3 can describe the measurements equally well. Furthermore, the calculated pressure gradient is significantly less sensitive to variations of parameter A_3 than of parameters A_1 and A_2 (which can easily be demonstrated by varying parameters in Eq. 9). Thus, we approximate the value of A_3 based on a simplified model of a two-dimensional (2-D) channel flow between two plates (see Figure 1). Assuming a stationary and developed flow, the force balance relates the pressure gradient $\partial p/\partial x$ and the wall shear stress τ_W as

$$\frac{\partial p}{\partial x} \cdot l \cdot b \cdot h = 2 \cdot \tau_W \cdot b \cdot l \tag{11}$$

The wall shear stress can be written as product of wall shear rate and the corresponding viscosity $\tau_W=\eta_W \cdot \dot{\gamma}_W$ with $\eta_W=\eta(\dot{\gamma}_W)$. If so, Eq. 11 leads to

$$\dot{\gamma}_W = \frac{1}{\eta_W}\frac{\partial p}{\partial x} \cdot \frac{h}{2} \tag{12}$$

Considering Eq. 8 and substituting the term in brackets with Eq. 10 results in

$$\dot{\gamma}_r = \frac{1}{\eta_r} \cdot \frac{\Delta p}{\Delta x} \cdot \frac{A_3}{A_2} \cdot D \tag{13}$$

Comparing the simplified two-plate model with the real situation of a twin-screw, and assuming, that $\dot{\gamma}_W$ and η_W are estimates for $\dot{\gamma}_r$ and η_r, Eqs. 12 and 13 yield the following approximation for A_3

$$A_3 \approx \frac{A_2 \cdot h}{2 \cdot D} \tag{14}$$

In this equation, the gap distance h is not known. In fact, the gap distance between the screw and the barrel in an extruder varies depending on the cross-sectional profile of the screws (see Figure 2). To create an average, the parameter h was estimated as ratio between the gap cross-section area A_{cr} (i.e., shaded area in Figure 2 top) and the gap length l_{gap} (estimated as the entire length of the lines shown in Figure 2 bottom). Parameter h was calculated as

$$h = \frac{A_{cr}}{l_{gap}} \tag{15}$$

The use of Eqs. 14 and 15 reduces the number of free parameters to two (A_1 and A_2), and the solution of the fitting problem is unique.

Temperature dependency

As expected, the melt temperature was not constant during our measurements. In addition to the expected dependence of the melt temperature on the screw speed, the melt temperature also slightly varied with the throughput. Due to the strong temperature dependency of the viscosity, we could

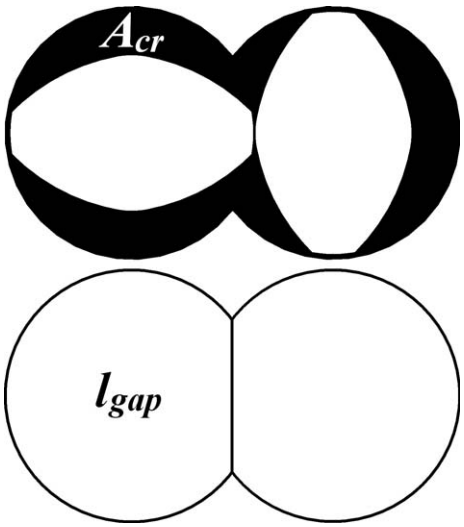

Figure 2. Schematic of gap cross-section area A_{cr} (top) and gap length l_{gap} (bottom).

Table 1. Menges Model Parameters

	Solid	Liquid
K_1 [bar cm^3/g]	29716	29519
K_2 [bar cm^3/g°C]	0.35526	1.1618
K_3 [bar]	1671.5	2614.4
K_4 [bar]	34326	34783
	Transition temperature	
K_8 [°C]	72.729	
K_9 [°C/bar]	0.020912	

not neglect this effect and incorporated the temperature dependency in the pressure characteristic of Kohlgrüber and Wiedmann,[5] using a temperature shift factor a_T in the Carreau model Eq. 5[31]

$$\eta(\dot{\gamma},T)=\frac{\eta_0\cdot a_T}{\left(1+\frac{|\dot{\gamma}|\cdot a_T}{\dot{\gamma}_{crit}}\right)^m} \tag{16}$$

The temperature shift factor in our case can be described by the Williams–Landel–Ferry (WLF) equation (often used for amorphous thermoplasts[30]), where C_1 and C_2 are material constants, that is,

$$a_T=\exp\left[\frac{-C_1\cdot(T-T_r)}{C_2+T-T_r}\right] \tag{17}$$

Using this and the approximation of A_3 (Eq. 14), the pressure-characteristic function Eq. 9 becomes

$$\frac{\Delta p_{C^*}}{\Delta x^*}=\frac{\Delta p}{\eta_0\cdot a_T\cdot n}\cdot\frac{D}{\Delta x}=\frac{A_2\cdot\left(1-\frac{\dot{V}^*}{A_1}\right)}{\left[1+\frac{A_2\cdot n\cdot a_T}{\dot{\gamma}_{crit}}\cdot\frac{h}{2D}\cdot\left|1-\frac{\dot{V}^*}{A_1}\right|\right]^m} \tag{18}$$

Eq. 10 remains unchanged. The representative viscosity is described by Eq. 16 for nonisothermal conditions.

Nonconveying elements

The proposed concept was shown by Kohlgrüber and Wiedmann[5] for actively conveying elements. Here, we derived a modification for nonconveying elements (e.g., kneading elements with 90° offset angle) for which parameters A_1 and A_2 are zero (i.e., the inherent conveying capacity and the ability to generate pressure are zero). In the limit of A_1 and A_2 going to zero in Eq. 18, the following equation is recovered, where $A_0=A_2/A_1$ for $A_1, A_2\to 0$

$$\frac{\Delta p_{C^*}}{\Delta x^*}=\frac{\Delta p}{\eta_0\cdot a_T\cdot n}\cdot\frac{D}{\Delta x}=\frac{-A_0\cdot\dot{V}^*}{\left[1+\frac{A_0\cdot n\cdot a_T}{\dot{\gamma}_{crit}}\cdot\frac{h}{2D}\cdot|\dot{V}^*|\right]^m} \tag{19}$$

Similarly, Eq. 8, including the approximation of A_3 (Eq. 14), and Eq. 10 can be used for nonconveying screw elements

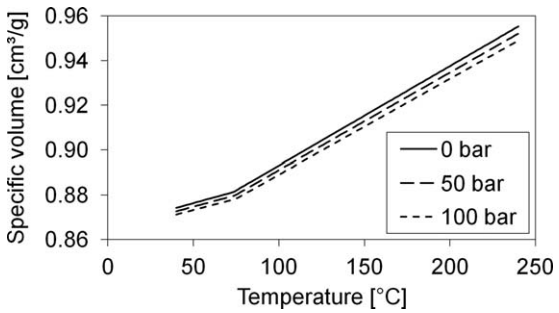

Figure 3. Specific volume as a function of temperature and pressure.

$$\dot{\gamma}_r=A_0\cdot n\cdot\frac{h}{2D}\cdot\dot{V}^* \tag{20}$$

$$\frac{\Delta p^*}{\Delta x^*}=\frac{\Delta p}{\eta_r\cdot n}\cdot\frac{D}{\Delta x}=-A_0\cdot\dot{V}^* \tag{21}$$

where the representative viscosity $\eta_r=\eta(\dot{\gamma}_r,T)$ is described by Eq. 16.

Materials

In our experiments, the pharmaceutical-grade matrix material Soluplus was used, which is a polyvinyl caprolactam-polyvinyl acetate-polyethylene glycol graft copolymer specifically designed for HME. Soluble in water and many organic solvents, it is well-suited as a solubilizer for poorly soluble drugs. More detailed information can be obtained from the manufacturer.[32] To evaluate our measurements, the equation of state and viscosity depending on the temperature and shear rate are required.

Equation of state

The equation of state of Soluplus was measured with a PVT-device of type PVT100 (SWO Polymertechnik GmbH, Germany) according to the standard ISO 17744.[33] Isobar-cooling with 6 K/min at five different pressure levels from 200 to 1200 bar was used. The measured data were fitted with the Menges model[34] (parameters K_1–K_4 are different for solid and liquid state), which describes the specific volume v [m^3/kg] depending on pressure p and temperature T

$$v=\frac{K_1}{p+K_4}+\frac{K_2\cdot T}{p+K_3}. \tag{22}$$

The transition temperature between solid and liquid states (in this case the glass transition temperature) depending on pressure p is described by

$$T_{trans}=K_8+K_9\cdot p \tag{23}$$

The parameters established through the experiments are provided in Table 1. The resulting dependence of the specific volume on temperature and pressure is shown in Figure 3. Clearly, the pressure impact is low (variation $<1\%$ between 0 and 100 bar) compared to the temperature variability (about 10% between 40 and 240°C). A discontinuity in the curves indicates the glass transition point of Soluplus (approximately 70°C[32]).

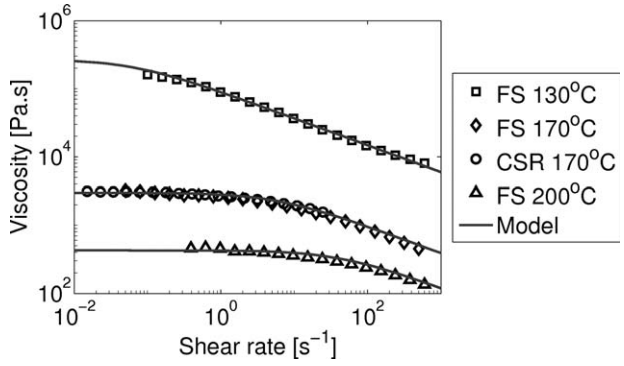

Figure 4. Viscosity over shear rate.

The shown measurements are frequency sweeps (FS) and a rotation test under controlled shear rate (CSR).

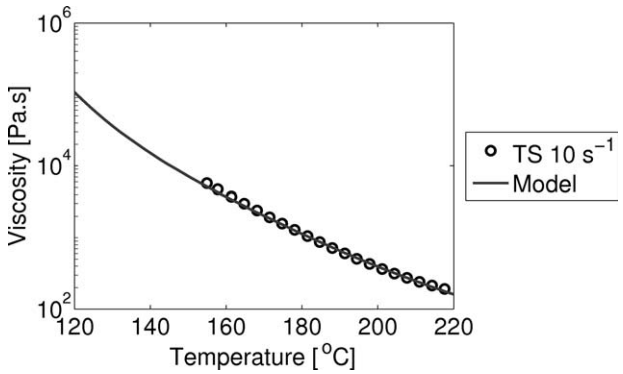

Figure 5. Viscosity over temperature.

The shown measurement is a temperature sweep (TS).

Melt viscosity

The viscosity of the Soluplus melt was measured with a MCR301 (Anton Paar, Austria) equipped with electric temperature control systems P-EDT400 and H-EDT400 and a cone-to-plate measurement body with a diameter of 25 mm and 1° cone angle. Different types of measurements were performed: three frequency sweeps (FS) at 130, 170, and 200°C, a rotation test with controlled shear rate (CSR) at 170°C, and a temperature sweep (TS) at 10 rad/s. Although the shear viscosity (i.e., the result of CSR tests) was required, FS tests are preferable as they allow a wider measurement range of angular frequency (and shear rate). As shown in Figure 4, FS and CSR at 170°C are in agreement, confirming the validity of the Cox–Merz rule[31], under which the result of the FS (complex viscosity depending on the angular frequency) is equal to the CSR result (shear viscosity depending on shear rate). In addition, to confirm the temperature dependency established via the FS at three different settings, a TS at a constant angular frequency of 10 rad/s was performed (Figure 5).

The model (Carreau and WLF equation, Eqs. 16 and 17) was fitted, and the yielding parameters are shown in Table 2. Calculated model curves vs. the measured data are shown in Figures 4 and 5. The measurements were in agreement with the data supplied by the manufacturer.[32]

Screw Characterization Experiments

Experiments were performed to measure the axial pressure gradient and material temperature for different throughputs, screw speeds, and screw element configurations. The extruder used was a ZSK 18 from Coperion (Germany) with a nominal screw diameter $D = 18$ mm. The characterization was performed for six different types of screw elements (all two-flighted), that is, two conveying screw elements termed "24/24" and "16/16" with different pitches of 24 and 16 mm, respectively, two kneading elements "KB 45/5/8" and "KB 45/5/8 LH" (45° offset angle, 5 discs, 8 mm length, right- and left-handed), a kneading element "KB 90/5/8" and a kneading element "KB 45/5/16". All elements are depicted in Figure 6. From the geometry of the cross section (Figure 2), a free cross-section area $A_{cr} = 187.8$ mm^2 was calculated. The gap length l_{gap} was 101.6 mm, leading to an average gap size $h = 1.847$ mm based on Eq. 15.

Two pressure sensors (melt pressure sensors from Gefran, Italy; I-Series, 0–35bar) were installed close to the screw end at an axial distance of $\Delta x = 43.2$ mm (see Figure 7). The built-in temperature sensors of the extruder are planar

Table 2. Viscosity Parameters

η_0	2999.9 Pa·s
$\dot{\gamma}_{crit}$	5.7852 s^{-1}
m	0.39489
T_r	170°C
C_1	10.7203
C_2	135.4020°C

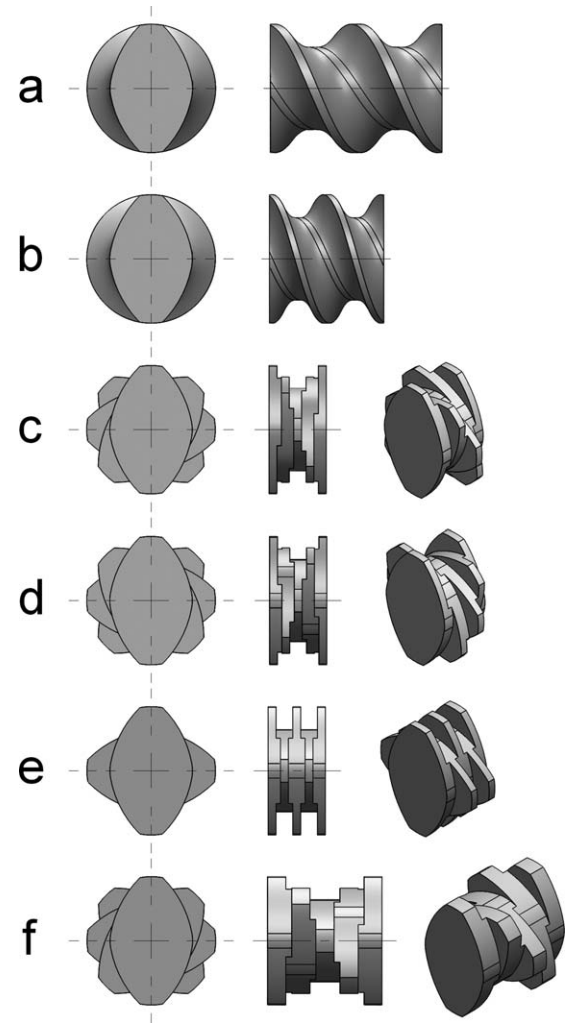

Figure 6. ZSK18 screw elements evaluated in our study.

(a) 24/24, (b) 16/16, (c) KB 45/5/8, (d) KB 45/5/8 LH, (e) KB 90/5/8, and (f) KB 45/5/16.

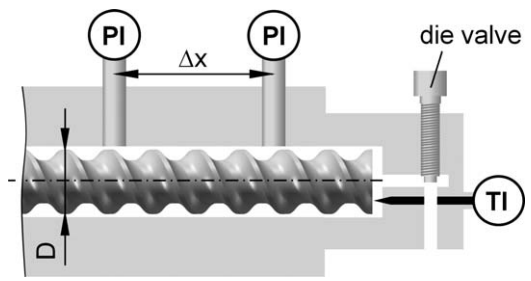

Figure 7. Experimental set-up.

PI is the pressure indicator and TI the temperature indicator.

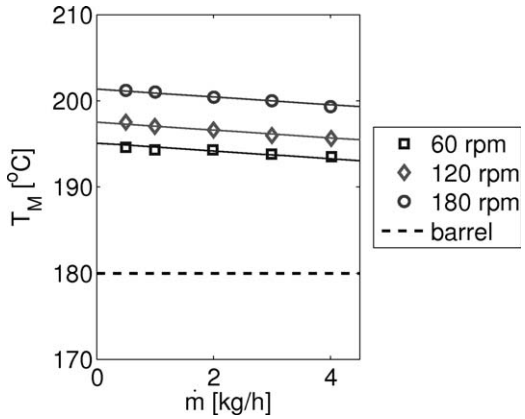

Figure 8. Melt temperature (points: measurement, lines: fit) over throughput at different screw speeds for the conveying screw element 24/24.

with the wall (similar to the pressure sensors) and their readings are strongly influenced by the barrel temperature. These sensors always measure some average of melt and barrel temperature. Thus, another temperature sensor (fast-response thermometer Thermapen from ETI Electronic Temperature Instruments, UK) was placed in the clearance volume directly behind the screw, which was the only option for inserting it directly in the melt flow. To avoid wall contact, the shaft of this additional temperature sensor was covered with a polytetrafluoroethylene (PTFE) casing. The measured temperature was significantly higher (approximately 3–10°C) than that indicated by the built-in temperature sensors, obviously significant viscous dissipation occurs. The screw section between both pressure sensors was configured with the screw element type being investigated. To ensure that the filled screw section extended over both pressure sensors, an adjustable die valve was constructed (Figure 7).

The barrel temperature was set to 180°C. Vacuum devaporization was used (200 mbar) to avoid foaming caused by moisture in Soluplus. The measurements were performed for three screw speeds (60, 120, and 180 rpm) and throughputs of 0.5–4 kg/h and 0.5–2 kg/h for the conveying and kneading elements, respectively. Each change of throughput or screw speed was maintained for at least 15 min to achieve a steady state before collecting data for 6 min using the SIPAT System (Siemens, Belgium) with a data acquisition rate of 5 s. As the measured pressure data showed significant oscillations, steady state in this case meant that the pressure difference was oscillating around a constant value over the considered time period. The measured temperature did not show oscillations and was recorded manually by the operator.

Results and Discussion

Measured data

The resulting data of the measured melt temperature and pressure gradient for the 24/24 screw element (Figure 6a) are shown in Figures 8 and 9. The melt temperature T_M was significantly higher than the barrel temperature due to the considerable amount of heat generated by viscous dissipation, even in the case of conveying elements. As expected, the temperature increased with the increasing screw speed due to greater dissipation and slightly decreased with increasing throughput due to the reduced axial pressure gradient (i.e., reduced viscous dissipation) and an increased cooling due to convective heat transport. The axial pressure gradient $\Delta p/\Delta x$ was averaged over 6 min for each measured data point, the error bars indicate the standard deviation of the observed oscillations. With increasing screw speed, the axial pressure gradient increased due to increased shear forces balanced by pressure gradients and decreased with increasing throughput due to a decreased backflow in the completely filled section, as also shown by the linear pressure-characteristic model for Newtonian fluids (Eq. 3). The dependency of the axial pressure gradient on the throughput becomes weaker with increasing screw speed. At 180 rpm, the pressure gradient was rather constant for the 24/24 screw element. This can be explained by the viscosity increase due to the corresponding temperature decrease of approximately 2°C, which dominates the slight decrease of the axial pressure gradient with increasing throughput expected due to the pressure characteristic (Note that also at 180 rpm, an inherent conveying capacity exists, i.e., a throughput, where the axial pressure gradient becomes zero. However, that throughput is relatively high at 180 rpm).

The data for all other screw elements were qualitatively similar and are not shown in detail. Specifically, we did not find a significant difference in the melt temperature for all investigated screw elements, indicating, that the heat generation by viscous dissipation is not significantly different, even for kneading elements. Note, that the local viscous dissipation rate is proportional to viscosity and shear rate squared ($q_{\mathrm{Diss}} = \eta \cdot \dot{\gamma}^2$). The dominating shear rates are mainly caused by the screw rotation and the gap distance between screws and barrel, which is equal for all investigated screw elements due to the invariant cross-section profile of the screws. In the case of kneading elements, the offset of the single discs causes additional gaps in the intermeshing region of the screws where high shear rates occur. However, this does not dominate the heat generation, as only a small amount of material is located in the crossover of offset regions and the intermeshing region.

Fitted model

The measurements were used to fit parameters A_1 and A_2 in Eq. 18 for all of the investigated screw elements and parameter A_0 in Eq. 19 for the nonconveying screw element KB 90/5/8. The specific volume per Eq. 22, which was

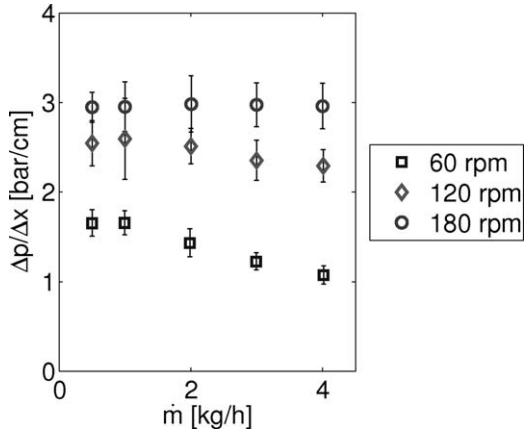

Figure 9. Axial pressure gradient over throughput at different screw speeds for the conveying screw element 24/24.

Table 3. Fitted Screw Parameters and Relative Variations Due to $h \pm 50\%$

Screw Element	A_1	A_2	A_3
24/24	0.3593 +15.3% / −7.6%	766.5 ±18.8%	39.33 +77% / −59%
16/16	0.2257 +6.4% / −3.4%	808.6 ±18.9%	41.49 +77% / −59%
KB 45/5/8	0.1545 +7.4% / −5.0%	259.1 ±10.2%	13.29 +65% / −55%
KB 45/5/16	0.1448 +4.8% / −3.6%	217.7 ±8.5%	11.17 +63% / −54%
KB 90/5/8	A_0 = 1214.4 ±2.9%		

required to convert mass throughput $\dot{m}$ [kg/h] into volumetric throughput $\dot{V}$ [m^3/h], was evaluated at the measured melt temperature T_M and the pressure $p = 0$, that is, the (small) pressure dependency was neglected (see Figure 3). The material parameters given in Tables 1 and 2 were used, and the temperature shift factor a_T per Eq. 17 was calculated based on the measured melt temperature T_M.

The fitted parameters for all of the investigated screw elements are shown in Table 3. In order to demonstrate the sensitivity of the fitted screw parameters A_0, A_1, and A_2 on the developed estimate of parameter h and A_3, the estimate h was varied by ±50% (1.847 mm ± 0.924 mm). The resulting deviations in A_0, A_1, A_2, and A_3 are shown by relative errors in Table 3. The values of parameter A_3 deviated in the range of 54–77%, while the corresponding deviations of A_0, A_1, and A_2 were in the range of 3, 3–15, and 8–19%, respectively. This indicates that deviations in A_0, A_1, and A_2, which were caused by deviations in A_3, were significantly lower than deviations in A_3, that is, the model is hardly sensitive to the estimated parameter A_3. As such, the used approximation is a valid approach and it can be expected that the data reported here allow the simulation of extruders and the prediction of their performance within technical accuracy ranges.

Using the determined parameters A_0, A_1, and A_2, the pressure-characteristic curves were calculated according to Eq. 18 for conveying elements and Eq. 19 for nonconveying element KB 90/5/8. The calculated curves describe changes in the dimensionless axial pressure gradient as a function of throughput and screw speed. The corresponding melt temperature is required for the evaluation of Eqs. 18 and 19 due to the temperature dependency of the viscosity, but cannot be predicted by the pressure-characteristic model. Thus, the melt temperature was determined from a linear fit of the measured temperature data $T_M(n, \dot{m}) = a_n - b \cdot \dot{m}$ (see solid lines in Figure 8, fitted parameters a_n and b are provided in Table 4).

A comparison between the calculated pressure-characteristic curves and the measured data is shown in Figures 10–15 for all investigated screw elements. The dashed lines represent the linear model of Newtonian fluids with axis intercepts A_1 and A_2 (calculated in Eq. 3). The discrepancy between that and the nonlinear curves fitting the measured data represents the effect of shear-thinning and temperature variations.

Clearly, the model fits the measured data well and is a good basis for extruder design and performance prediction. The model fit is better for the conveying screw elements 24/24 (Figure 10) and 16/16 (Figure 11) than for the kneading elements (Figures 12–15). This can be explained by the stronger relative pressure oscillations observed for the kneading elements (represented by error bars). The ratio of the inherent conveying capacity (i.e., parameter A_1) for both of the investigated conveying screw elements 0.3593/0.2257 = 1.59 is comparable with the ratio of their pitch 24/16 = 1.5. This is in agreement with the data reported by Kohlgrüber et al.[29], who stated that A_1 is approximately proportional to the screw pitch. Both A_1 parameters are comparable to the approximation calculated in Eq. 4 (0.3864 and 0.2576). In contrast, A_2 of the 24/24 and 16/16 are relatively similar, that is, the generated pressure gradient at zero throughput is not significantly different. Kohlgrüber and Wiedmann[5] demonstrated that A_2 generally increases with the decreasing pitch, except for cases when there is a large gap between the screw and the barrel (typical for relatively small machines, such as ZSK 18 that we used).

Parameters A_1 and A_2 are significantly lower for the kneading elements KB 45/5/8 (Figure 12) and KB 45/5/16 (Figure 13) than for the conveying elements due to the geometry of the kneading elements (Figure 6) with discontinuous steps rather than a smooth surface that reduces the conveying effect and pressure build-up. KB 45/5/16 has a slightly decreased A_1 and A_2 compared to KB 45/5/8, that is, the stretched geometry of KB 45/5/16 resulted in reduced conveying and pressure build-up.

The measured data of the screw element KB 45/5/8 LH were not fitted, as they should be identical to the pressure characteristic of KB 45/5/8 except for the inversed direction (negative throughput) due to its backward conveying effect (also see the corresponding literature[5,11]). The data points for KB 45/5/8 LH and KB 45/5/8 are shown together in Figure 14. Although the data approximately match at zero throughput, the axial pressure gradient of KB 45/5/8 LH showed an unexpected discrepancy compared to the fitted curves of KB

Table 4. Fitted Temperature Parameters

	a_n [°C]			
Screw element	60 rpm	120 rpm	180 rpm	b [°C.h/kg]
24/24	195.05	197.48	201.33	0.4545
16/16	191.73	195.88	200.48	0.3566
KB 45/5/8	194.02	198.33	200.97	0.3360
KB 45/5/16	193.91	199.97	202.74	1.0076
KB 90/5/8	195.97	199.90	203.53	0.7424

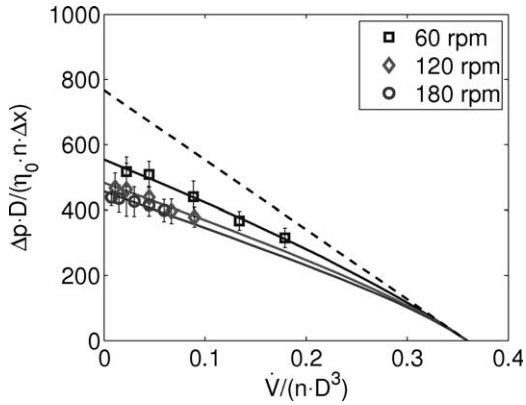

Figure 10. Pressure characteristic based on η_0 for the conveying screw element 24/24.

Dots: measurements, solid lines: model for Soluplus, dashed line: model for Newtonian fluids.

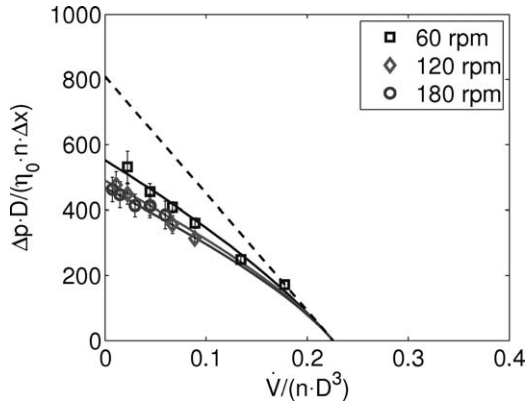

Figure 11. Pressure characteristic based on η_0 for the conveying screw element 16/16.

Dots: measurements, solid lines: model for Soluplus, dashed line: model for Newtonian fluids.

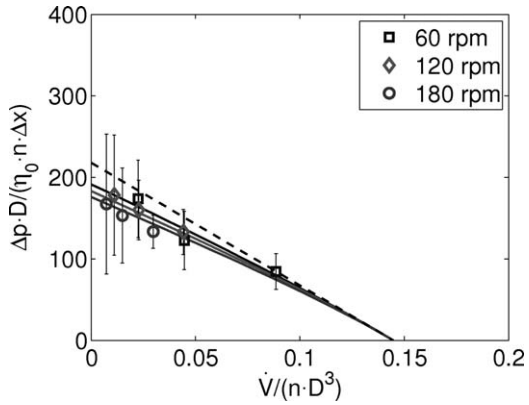

Figure 13. Pressure characteristic based on η_0 for the kneading element KB 45/5/16.

Dots: measurements, solid lines: model for Soluplus, dashed line: model for Newtonian fluids.

45/5/8, even a decreasing axial pressure gradient with increasing negative throughput in some regions.

As expected, the kneading element KB 90/5/8 (Figure 15) had a pressure-characteristic line passing the origin as its geometry does not cause a preferred conveying direction and is thus nonconveying. The curve slope was similar to the other kneading elements, meaning that the change in the pressure drop with varying throughput was similar.

The resulting linear pressure-characteristic curves of all of the investigated screw elements are compared in Figure 16. For a clear graphical representation, the dimensionless axial pressure gradient $\Delta p^*/\Delta x^* = \Delta p{\cdot}D/(\eta_r{\cdot}n{\cdot}\Delta x)$ according to Eq. 10 (Eq. 21 for nonconveying elements) was used, in contrast to $\Delta p_C^*/\Delta x^* = \Delta p{\cdot}D/(\eta_0{\cdot}n{\cdot}\Delta x)$ as used for Figures 10–15. The obvious difference is the shear-rate-dependent representative viscosity η_r (in contrast to η_0), which leads to a linear correlation, as the shear-thinning effect of the melt rheology is incorporated in η_r. Thus, all data points of a screw element are located along the pressure characteristics for Newtonian fluids in Figure 16 which is independent of the screw speed.

Although the relative oscillations of the kneading elements were significantly higher than those of the conveying elements, the absolute oscillations of the dimensionless pressure gradient were similar for the investigated screw elements (see Figure 16). The cross-section profile of the screw elements was equal for all considered elements. This indicates that the observed oscillations of the axial pressure gradient are caused by the rotation of the screws, which led to pressure maxima in front of and minima behind the screw flights with respect to the rotational direction (this conjecture, however, cannot be proven based on the shown data, as the data acquisition rate of 5 s does not resolve the circulation time of the screws). However, this effect has been shown by 3-D simulations of twin screws[5] for the pressure distribution over the cross section.

Summary and Conclusions

This work presents the first detailed experimental characterization of completely filled screw elements for pharmaceutical HME with Soluplus on a co-rotating twin-screw extruder. Specifically, the pressure-characteristic (i.e., the correlation between the axial pressure gradient and the volumetric throughput in a completely filled screw section) was measured at different screw speeds and for different screw elements. The required rheological properties and the specific volume of Soluplus were determined in detail the first time by precise

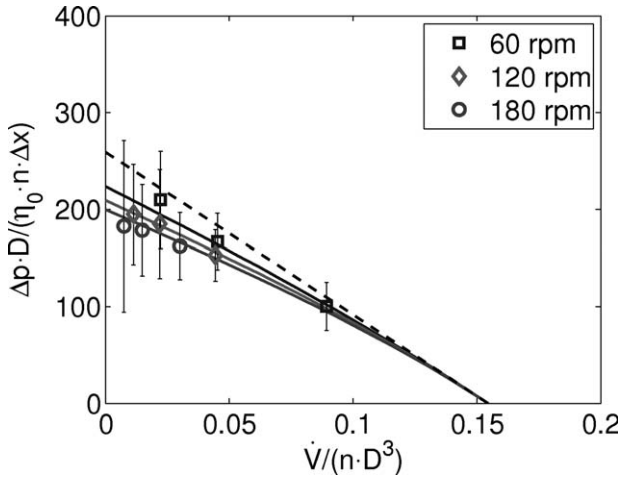

Figure 12. Pressure characteristic based on η_0 for the kneading element KB 45/5/8.

Dots: measurements, solid lines: model for Soluplus, dashed line: model for Newtonian fluids.

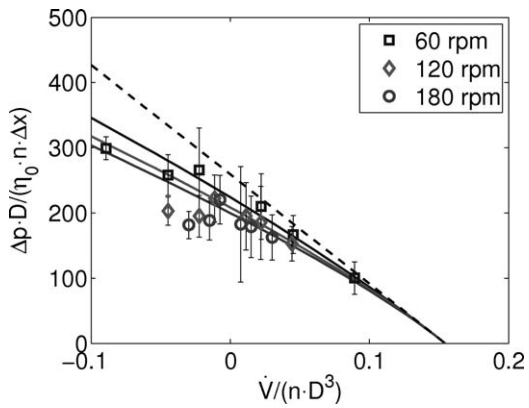

Figure 14. Pressure characteristic based on η_0 for the kneading element KB 45/5/8 together with KB 45/5/8 LH.

Dots: measurements, solid lines: model for Soluplus, dashed line: model for Newtonian fluids.

measurements and described via the Carreau model combined with the WLF equation, and the Menges model, respectively. The pressure-characteristic model[5,10] was fitted to describe the measured data. As fitting of three parameters was found to be an underdetermined problem, an approximation of the parameter A_3, which has a lower impact on the results than parameters A_1 and A_2, was developed based on a mechanistic understanding of the pressure-driven flow. The effect of the approximation was significantly lower for A_1 and A_2 than for A_3, that is, deviations in A_1 and A_2 were lower than deviation in A_3 introduced by the approximation. As it was established that the melt temperature was not constant for variable throughput and screw speed, a temperature dependency was included into the model using a linear fit of the measured temperature over the throughput.

The results show significantly different pressure-characteristic curves and corresponding screw parameters for the investigated screw elements. A comparison of the screw parameters for the different elements confirm the expected tendencies, such as the proportionality of the inherent conveying capacity and the screw pitch of conveying screw elements, as well as the same axial pressure gradient for right- and left-handed elements of the same type (i.e., inverse conveying direction) at zero throughput.

More detailed studies (e.g., via numerical simulations) are required to investigate why the backward-conveying kneading element KB 45/5/8 LH deviated from the model curves of element KB 45/5/8 and, in some regions, had decreased pressure gradients at increased throughputs. Extensive 3-D simulations (e.g., CFD) of the investigated screw elements are necessary to confirm the determined screw parameters and pressure-characteristic curves and to analyze the developed approximation of A_3. This is currently the aim of our work.

Although we used only one type of material and one type of extruder for our measurements, the applicability of the results to other cases is supported by the following reasons. The dimensionless formulation of the model leads to scale invariance, that is, geometrically similar screw elements at different length scales have identical screw parameters. Moreover, the screw parameters are invariant of the melt viscosity in the creeping flow regime (which is typically the case for the highly viscous materials used in HME). Both statements were experimentally verified for single-screw extruders by Pawlowski[10]. Consequently, the reported screw parameters can be applied to different screws, if they are geometrically similar. The used pressure-characteristic model was developed from the linear model for Newtonian fluids. Incorporating the melt rheology (the Carreau model in our case), it can be used for non-Newtonian fluids. However, the screw parameters A_1 and A_2 always characterize the axis intercepts of the linear model for Newtonian fluids. Thus, A_1 and A_2 are independent of the used material. This was not shown in our present work. Numerical studies with different rheologies could verify this assumption and open a way of determining such parameters for other types of screw elements without performing experiments.

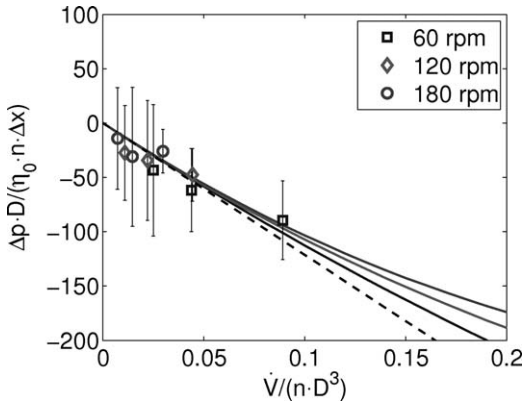

Figure 15. Pressure characteristic based on η_0 for the kneading element KB 90/5/8.

Dots: measurements, solid lines: model for Soluplus, dashed line: model for Newtonian fluids.

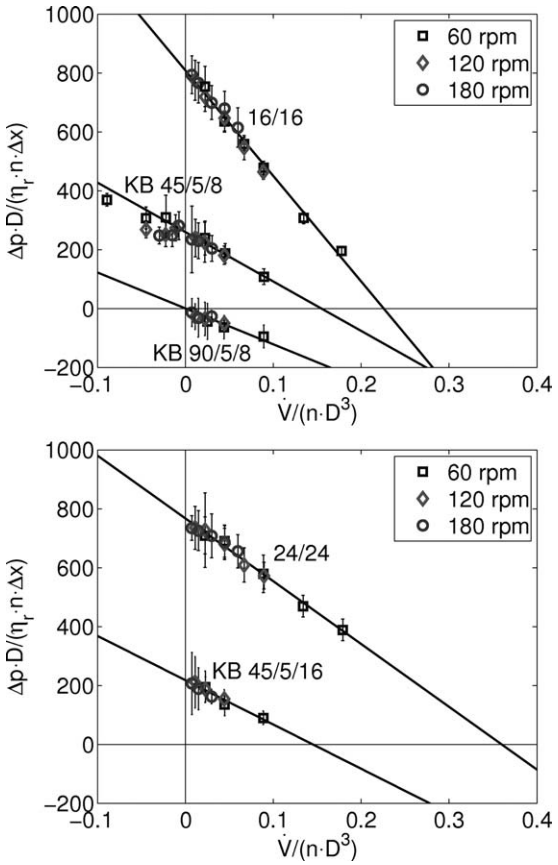

Figure 16. Pressure-characteristic curves based on η_r for all of the investigated screw elements in comparison (dots: measurements, lines: model).

The determined parameters confirm an essential premise for a 1-D model of a co-rotating twin-screw extruder, which cannot predict the transport processes caused by the screw elements based directly on the 3-D geometry. Using the obtained screw parameters, such a model can predict process variables (e.g., filling ratio, pressure and melt temperature along the twin screw). Although the shown experiments have exclusively been performed for a completely filled screw section, the results can be used to estimate filling ratio and pressure in partially filled screw sections. Axial pressure gradients in partially filled screw sections are zero due to the connected gas phase. The dependency of the filling ratio on the throughput can be estimated linearly[5] $f = \dot{V}/(A_1 \cdot n \cdot D^3)$, that is, filling ratio = 0 at throughput = 0, filling ratio = 1 at

the inherent conveying capacity. Moreover, based on the calculated flow rates along the screw such a 1-D model can predict residence time distributions, that is, characterize the mixing performance of the process.

Acknowledgments

We thank BASF (Ludwigshafen, Germany) for providing Soluplus and MAAG-Automatic Pelletizing Systems (Groostheim, Germany) and Reinhardt-Karsten Mürb for providing ZSK18 screw elements. Furthermore, we acknowledge Johann Grubbauer for support in assembling the die valve and the temperature sensor, Sarah Windhab for help with the rheological measurements, Markus Gamsriegler, Mario Unterreiter, and Daniel Kaiser for their support during the experiments and Daniel Markl for his assistance with the SIPAT system. Moreover, the University of Leoben, Department for Polymer Engineering and Science, is acknowledged for support in the PVT measurements.

Notation

Latin symbols

A_0 = screw parameter for nonconveying elements, -
A_1, A_2 = screw parameters for conveying elements, -
A_3 = empirical shear rate parameter, -
a_T = temperature shift factor (Carreau model, WLF equation), -
C_1, C_2 = parameters of the WLF equation
D = nominal screw diameter, m
h = gap distance, m
K_1, K_2, K_3, K_4, K_8, K_9 = parameters of the Menges model
$\dot{m}$ = mass throughput [kg/s]
m = Carreau exponent, -
n = screw speed, s^{-1}
p = pressure, Pa
$\frac{\Delta p^*}{\Delta x^*}$ = dimensionless axial pressure gradient based on the representative viscosity η_r or Newtonian viscosity η, -
$\frac{\Delta p_{C^*}}{\Delta x^*}$ = dimensionless axial pressure gradient based on the zero-shear rate viscosity η_0 (Carreau model), -
Re = Reynolds number, -
T = temperature, °C
T_M = measured melt temperature, °C
T_r = reference temperature (WLF equation), °C
T_S = screw pitch, m
T_{trans} = transition temperature (Menges model), °C
$\dot{V}$ = volumetric throughput, m^3/s
$\dot{V}^*$ = dimensionless volumetric throughput, -
v = specific volume, m^3/kg
x = axial coordinate, m

Greek letters

$\dot{\gamma}$ = shear rate, s^{-1}
$\dot{\gamma}_{crit}$ = critical shear rate (Carreau model), s^{-1}
$\dot{\gamma}_r$ = representative shear rate, s^{-1}
η = dynamic viscosity, Pas
η_0 = zero-shear-rate viscosity (Carreau model), Pas
η_r = representative viscosity, Pas
ρ = density, kg/m^3
τ_W = wall shear stress, Pa

Literature Cited

1. Kleinebudde P. Pharmazeutisches Produktdesign: Gezielte Freisetzung von Wirkstoffen durch unterschiedliche Extrusionstechniken. *Chemie Ingenieur Technik*. 2011;83(5):589–597.
2. Ghebre-Sellassie I, Martin C. Pharmaceutical Extrusion Technology. New York: Marcel Dekker, 2003.
3. Breitenbach J. Melt extrusion: from process to drug delivery technology. *European Journal of Pharmaceutics and Biopharmaceutics*. 2002;54(2):107–117.
4. Repka MA, Battu SK, Upadhye SB, Thumma S, Crowley MM, Zhang F, Martin C, McGinity JW. Pharmaceutical applications of hot-melt extrusion: Part II. *Drug Develop Ind Pharm*. 2007;33(10): 1043–1057.
5. Kohlgrüber K, Wiedmann W. Co-Rotating Twin-Screw Extruders. Munich: Carl Hanser Verlag, 2008.
6. Yacu WA. Modelling a twin screw co-rotating extruder. *J Food Eng*. 1985;8:1–21.
7. Meijer HEH, Elemans PHM. The Modeling of Continuous Mixers. Part I: The Corotating Twin-Screw Extruder. *Polym Eng Sci*. 1988; 28(5):275–290.
8. White JL, Chen Z. Simulation of non-isothermal flow in modular co- rotating twin screw extrusion. *Polym Eng Sci*. 1994;34(3):229–237.
9. Potente H, Hanhart W. Design and processing optimization of extruder screws. *Polym Eng Sci*. 1994;3(11):937–945.
10. Pawlowski J. *Die Ähnlichkeitstheorie in der physikalisch-technischen Forschung*. Berlin/Heidelberg/New York: Springer-Verlag, 1971.
11. Szydlowski W, White JL. An improved theory of metering in an intermeshing corotating twin-screw extruder. *Adv Polym Technol*. 1987;7(2):177–183.
12. Potente H, Fornefeld A, Michel P, Wittemeier R. Analyse und Berechnung der Strömungsvorgänge im zylindrischen Scherspalt von Plastifizieraggregaten. *Rheological Acta*. 1987;26(2):193–199.
13. Wang Y, White JL. Non-newtonian flow modelling in the screw regions of an intermeshing corotating twin screw extruder. *J Non-Newtonian Fluid Mech*. 1989;32:19–38.
14. Barrera MA, Vega JF, Martínez-Salazar J. Three-dimensional modelling of flow curves in co-rotating twin-screw extruder elements. *J Mater Process Technol*. 2008;197:221–224.
15. Potente H, Koch M. Residence time behavior in grooved-barrel extruders. *Adv Polym Technol*. 1989;9(2):119–127.
16. De Ruyck H. Modelling of the residence time distribution in a twin screw extruder. *J Food Eng*. 1997;32:375–390.
17. Giudici R, Nascimento CAO, Beiler IC, Scherbakoff N. Transient experiments and mathematical modeling of an industrial twin-screw extruder reactor for Nylon-6,6 polymerization. *Ind Eng Chem Res*. 1997;36(9):3513–3519.
18. Puaux J., Bozga G, Ainser A. Residence time distribution in a corotating twin-screw extruder. *Chem Eng Sci*. 2000;55:1641–1651.
19. Baron R, Vauchel P, Kaas R, Arhaliass A, Legrand J. Dynamical modelling of a reactive extrusion process: focus on residence time distribution in a fully intermeshing co-rotating twin-screw extruder and application to an alginate extraction process. *Chem Eng Sci*. 2010;65:3313–3321.
20. Choulak S, Couenne F, Le Gorrec Y, Jallut C, Cassagnau P, Michel A. Generic dynamic model for simulation and control of reactive extrusion. *Ind Eng Chem Res*. 2004;43(23):7373–7382.
21. Zagal A, Vivaldo-Lima E, Manero O. A mathematical model for the reactive extrusion of methyl methacrylate in a co-rotating twin-screw extruder. *Ind Eng Chem Res*. 2005;44(26):9805–9817.
22. Puaux J-P, Cassagnau P, Bozga G, Nagy I. Modeling of polyurethane synthesis by reactive extrusion. *Chem Eng Process*. 2006;45: 481–487.
23. Bertrand F, Thibault F, Delamare L, Tanguy PA. Adaptive finite element simulations of fluid flow in twin-screw extruders. *Comput Chem Eng*. 2003;27:491–500.
24. Potente H, Többen WH. Improved design of shearing sections with new calculation models based on 3D finite-element simulations. *Macromol Mater Eng*. 2002;287(11):808–814.
25. Pokriefke G. Numerical simulation of 2d fluid flow in an partially filled simplified extruder model. *Proc Appl Math Mech*. 2003;3:418–419.
26. Ficarella A, Milanese M, Laforgia D. Numerical study of the extrusion process in cereals production: Part I. Fluid-dynamic analysis of the extrusion system. *J Food Eng*. 2006;73:103–111.
27. Rodríguez EO. Numerical simulations of reactive extrusion in twin screw extruders, Ph.D. Thesis, University of Waterloo, Canada, 2009.
28. Cleary PW, Robinson M. Understanding viscous fluid transport and mixing in a twin screw extruder. In: 8th International Conference on CFD in Oil & Gas, Metallurgical and Process Industries. Trondheim, Norway: SINTEF/NTNU, 2011:1–8.
29. Kohlgrüber K, Hepperle J, König T, Conzen C, Bierdel M, Kirchhoff J, Thiele H. Optimierter Betrieb und Scale-up von Doppelschnecken-Extrudern. In: Seminar Handout. Leverkusen, Germany: VDI Wissensforum, 2012.

30. Rauwendaal C. Polymer Extrusion, 4th ed. Munich: Hanser Publishers; 2001.
31. Mezger T. Das Rheologie-Handbuch. Hannover: Curt R. Vinzentz Verlag, 2000.
32. Kolter K, Karl M, Gryczke. Hot-Melt Extrusion with BASF Pharma Polymers; Extrusion Compendium, 2nd ed. Ludwigshafen: BASF, 2012.
33. Germuth A. Untersuchungsbericht: Messung von thermodynamischen Stoffdaten an einem Copolymer der Type Soluplus. Leoben: Montanuniversität Leoben, Lehrstuhl für Kunststoffverarbeitung, 2012.
34. Huilier DGF. Modeling of injection mold post-filling: a review and some critical problems to solve. *J Polym Eng*. 1990;9(4):237–302.

Manuscript received Feb. 26, 2013, and revision received Jun. 7, 2013.